Scientia Iranica B (2014) 21(1), 109–118

SCIENTIA IRANICA

Sharif University of Technology
Scientia Iranica
Transactions B: Mechanical Engineering
www.scientiairanica.com

Simulations of particle filtration and tracking in an electrical field

A. Sedaghat* **and A.H. Mohamadzadeh**

Department of Mechanical Engineering, Isfahan University of Technology, Isfahan, P.O. Box 84156-83111, Iran.

Received 22 October 2011; received in revised form 14 July 2013; accepted 13 August 2013

KEYWORDS
Particle/gas flow;
Numerical simulation;
Electrical filter;
Powder coating.

Abstract. The movement of charged particles in an electrical field is of practical importance in filtration efficiency and in electrostatic coating. In this paper, both of these applications have been investigated computationally. For the case of filtration, a mathematical model is introduced for the electric filter, which is made of split type fibers. The filter was assumed to be composed of rectangular fibers arranged in a staggered array field. Simulation was conducted to study filtration efficiency. Single fiber efficiencies under various filtration conditions were calculated and compared with results obtained from semi-empirical expressions. In the electrostatic powder painting, gas flow and particle flow fields inside a coating booth under given operating conditions are considered and the effects of particle size on their trajectories are studied. Steady state turbulent gas flow is simulated by solving incompressible Navier-Stokes equations and the standard $k-\varepsilon$ turbulence model. The discrete phase of particles is modeled based on the Lagrangian approach. In both cases studied here, the flow field and the collection mechanisms were accurately simulated experimental observations.

1. Introduction

Electrostatic powder spray painting is of significant industrial interest, since it offers many advantages and great flexibility. The movement of charged particles in an electrical field has practical use in powder collection and treatment processes for making a better filter. Electret filters are often utilized in industrial fields that require high collection efficiency with low flow resistance. An electret filter contains fibers that have a quasi-permanent electric charge which aids in capturing particles. Electret fiber can be classified into spun and split types. Typically, a split fiber has a tape-like cross-section and carries a high bipolar charge.

In this study, CFD simulations are made for electrostatic powder painting, in which the gas and particle flow fields inside a coating booth are considered under different operating conditions. The effects of particle size on the trajectories are studied by solving steady state turbulent incompressible gas flow using the standard $k-\varepsilon$ turbulence model. The discrete phase of particles is modeled based on the Lagrangian approach. A mathematical model is introduced for the electret filter, which is made of split type fibers. Simulation was also conducted to study filtration efficiency. The filter was assumed to be composed of rectangular fibers arranged in a staggered array field.

In this paper, the literature review is given next. Then, the problem description is given in Section 3, where electrostatic filtration and electrostatic powder coating are explained. In Section 4, the governing equations are presented, which include filtration model, equations for particles in filtration, the electrostatic field, and particles in the electrostatic field. Section 5 shows the results of the simulations, which express

*. *Corresponding author. Tel.: +98 311 3912667; Fax: +98 311 391 2628*
E-mail addresses: sedaghat@cc.iut.ac.ir (A. Sedaghat), a.mohamadzadeh@mech.iut.ac.ir (A.H. Mohammadzadeh)

filtration efficiency and powder coating performances. Finally, in Section 6, conclusions of this study are drawn and scope for further study is discussed.

2. Literature review

Many investigators have carried out similar experiments to study the effects of different parameters on the collection efficiencies of electret filters. Some experiments were conducted, including filter materials loaded with sanding wood dust, in Welling et al. [1] in 2008, and nanofiber layers by Leung et al. [2], in 2009.

In 2010, Li and Jo [3] studied a bundle-type electret filter in the Mechanical Ventilation and Air-Conditioning (MVAC) system of a metro-subway, experimentally, which demonstrated a higher filter quality than mechanical filters. Some custom painting process was defined, in 2010 by Quadrini et al. [4], for metal sheets by means of powder coating and localized heating.

The removal of ultrafine particles (UFP) from indoor air using Portable Air Cleaners (PAC) of various technologies has been studied experimentally by Sultana et al. [5] in 2011. They found that high-efficiency particulate air and electrostatic precipitators have the best performance, particularly with an electret based PAC.

In 2012, the foam fractionation method was applied by Atsushi Tanaka et al. [6] for nanocellulose to prevent the flow of coarse particles along water, where the foam acts like a filter. The advantage of the method was reported as no risk of clogging, which could be a big problem for conventional filters or screens.

In a few studies, numerical simulation was also involved [7-9], while, in others, useful expressions were derived for evaluation of overall collection efficiency and for evaluation of single fiber efficiency due to individual capturing mechanisms, such as dielectrophoretic and electrophoretic capture mechanisms [10-13].

In addition, simulations for the flow field, particle trajectory and particle deposition have also been investigated by Brown [14-15] in 1979 and 1981, respectively, Kanaoka et al. [11] in 1998 and Oh et al. [16] in 2001. As far as electret fibers are concerned, the numerical models were mainly for circular fibers [10,11,16] or based on circular cross-section assumption.

In 2002, Böttner and Sommerfeld [17] used Computational Fluid Dynamics (CFD) to simulate a complete electrostatic powder coating process under the Laplace condition, using two types of corona spray gun: a slit nozzle and a round nozzle with a dispersion cone, and two types of coating parts: a flat plate and a tube. The results agree well with the experimental data for both the particle velocity field and the coating layer thickness. However, they ignored the effect of space charge on the electrostatic field, and the effect of ion wind, generated by collisions between ions and molecules with neutral charge, on the airflow field. In 2002, Ye et al. [18] simulated the electrostatic powder coating process using the commercial CFD code, FLUENT v5.2. A corona spray gun was used. They considered the influence of space charge due to charged particles on the overall electrostatic field, but ignored the effect of ion wind. Direct interaction between particles and the effect of particle motion on the continuous phase were neglected. The numerical results were compared with the experimental data and good agreement was found for air velocities and coating layer thickness. Later, in 2003, Ye and Domnick [19] extended the above model to consider the space charge due to the free ions, but did not include the space charge due to charged particles, and the effect of particle motion on the continuous phase. In 2006, Li et al. [20] computationally studied air-particle two-phase flows inside a powder coating booth. They solved three dimensional Navier-Stokes equations, with a standard $k-\varepsilon$ turbulence model for the continuous phase (the air) and the discrete second phase (the particles), in a Lagrangian frame of reference.

Prediction of accurate trajectories of biological particles has recently been considered for the efficient design of micro devices for dielectrophoretic manipulation. In 2013, Juberya and Dutta [21] used an efficient numerical based approach on a distributed Lagrange multiplier based Fictitious Domain (FD) for flow field and the motion of biological particles, and a multi-domain method for electric potential. The capability of their model was demonstrated by simulating the trajectories of two biological particles (cells) of the same geometry and size but different dielectric properties in a micro device.

3. Problem descriptions

3.1. Electrostatic filtration

To solve the flow field inside a filter, a staggered array model, initially proposed in 1992 by Fardi and Liu [22,23], is used, in which infinitely long parallel rectangular fibers are placed perpendicular to the main flow direction, as schematically shown in Figure 1. Space between the fibers is decided according to packing density, α, of the filter. In 2002, Chen et al. [24] solved the two-dimensional flow field through a staggered array of fibers with a rectangular cross section. The same model is adopted here. In this model, the flow is assumed to be periodic within the domain along the flow direction, and thus, the flow field inside the module AEFD provides a typical representation of the flow pattern through the filter. Since one half of the periodic module, ABCD, is a symmetrical inversion of the other half, BEFC, the problem can be simplified by considering either half of

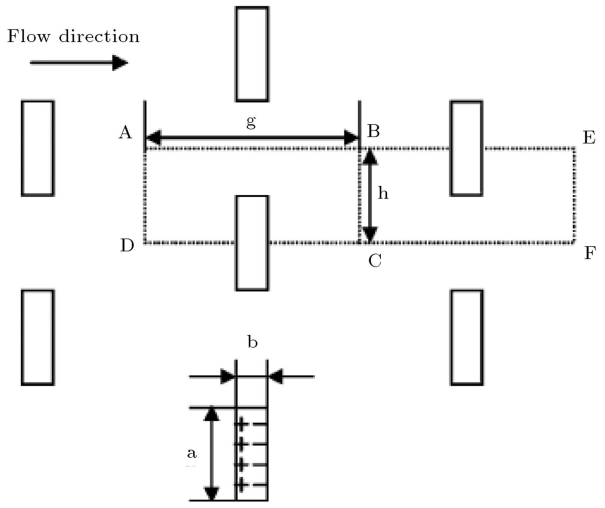

Figure 1. Scheme of staggered fibers' array, vertical fiber arrangement.

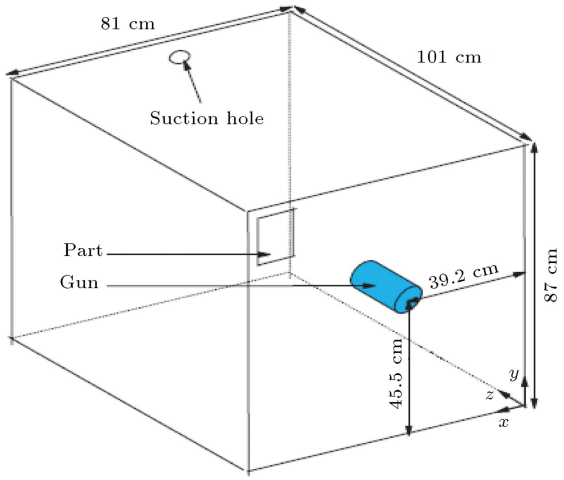

Figure 2. Coating booth dimensions and spray gun position.

the periodic module. Flow inside cell ABCD is solved by numerically integrating the Navier-Stokes equations by applying appropriate boundary conditions.

3.2. Electrostatic powder coating

A typical powder coating process consists of a fluidized bed hopper, a powder transport line from the hopper to the spray gun, an electrostatic spray gun, a coating booth and the work piece to be coated. The dimensions of the coating booth and the relative positions of the gun and coating part are shown schematically in Figure 2. A 3 cm diameter suction hole at the top wall of the booth, as shown in Figure 2, was used to maintain negative pressure inside the booth. So, the powder particles will stay inside the booth. The back wall functions as a particle collector.

The 15 cm long corona spray gun, as shown in Figure 3, was used to spray the powder particles. The air fluidized powder flows through the annular

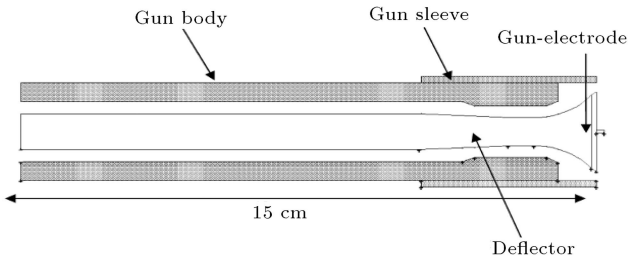

Figure 3. Cross-sectional view of Nordson corona spray gun.

space between the central trumpet-shaped cylindrical deflector and the outer gun body.

The adjustable gun sleeve, which is used to adjust the powder flow pattern, was kept throughout the study in the same position, as shown in Figure 2. The thin wire electrode, which is mounted at the center of the deflector plate, was applied with 50 kV to generate the electrostatic field between the gun and the grounded coating part. The radius of the tip of the electrode was 0.3 mm. The 7.6 cm × 13.2 cm sized coating part was mounted 26 cm downstream of the gun-tip. The air fluidized powder spray flow inside the coating booth was simulated as a two-phase flow, with air as the continuous and particles as the dispersed phase. In the present study, the particle volume fraction is less than 0.1% and, hence, the process is a dilute gas-solid two-phase flow in the regime of two-way coupling. The two-way interactions between the gas and particulate phases are included in the drag source terms in the momentum equations for both phases. The effect of possible particle-particle interaction on the flow is neglected. The effect of space charge, due to free ions on the electrostatic field, was included in the transport equation for the electrostatic field. The effect of ion wind on the airflow field, which could have a strong influence near the gun electrode region, is ignored, which means the electrostatic field affects the airflow only through its influence on particle trajectories by adding an electrostatic body force on particles.

4. Governing equations

4.1. Filtration model

To determine the electrostatic collection mechanisms, it is necessary to know the electrostatic field around each electret fiber. For loosely packed filters (packing density $a < 0.1$), the interaction between electrostatic fields generated by individual fibers can be neglected [25]. Surface charge on an electret fiber is considered an arrangement of many parallel line charges of infinite extent along its axis [26]. Accuracy is ensured when the line pair number is large enough. Figure 4 illustrates the model; the electrostatic field at any point around the fiber can be determined by the

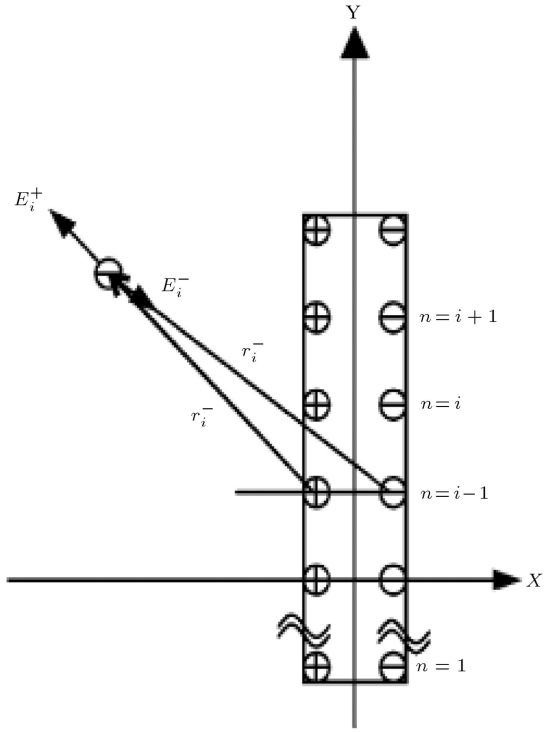

Figure 4. Simulation of electrostatic field at certain point around a split fiber.

sum of electrostatic fields generated by each of the line charge pairs.

$$\vec{E} = \sum_{i=1}^{n} \vec{E}_i^+ + \vec{E}_i^- = \frac{\lambda}{2\pi\varepsilon_0} \sum_{i=1}^{n} \frac{r_i^+}{(r_i^+)^2} - \frac{r_i^-}{(r_i^-)^2}, \quad (1)$$

where n is the number of line charge pairs, ε_0 is space permittivity, r_i^+ and r_i^- are displacement vectors;

$$\lambda = \frac{b\sigma}{n\varepsilon_f}. \quad (2)$$

ε_f is the dielectric constant of fiber material and $\varepsilon_f = 5$.

4.2. Particles in filtration

In filtration, the Coulombic force, $\vec{F}_C$, for a singly charged particle and the polarization force, $\vec{F}_P$, for a neutral particle can be expressed as:

$$\vec{F}_C = e\vec{E}, \quad (3)$$

$$\vec{F}_P = \frac{\pi}{4}\left(\frac{\varepsilon_P - 1}{\varepsilon_P + 2}\right)\varepsilon_0 d_P^3 \,\mathrm{grad}|\vec{E}|^2, \quad (4)$$

$$\vec{F}_e = \vec{F}_P + \vec{F}_c. \quad (5)$$

But, for a neutral particle, $\vec{F}_P$ is zero. Trajectories of particles that are released from the cell inflow surface, AD (Figure 1), are traced and recorded as they flow through the cell domain, ABCD. The ratio of number of particles captured to total number of particles released, after being normalized by the height of the fiber, will yield the single fiber efficiency:

$$\eta = \frac{\text{capture particle number}}{\text{total particle number}} \frac{2h}{a}, \quad (6)$$

in which a is the fiber height, i.e. the thickness of the fiber facing the incoming flow. The trajectory of a particle can be determined by solving the equation of motion of the particle as it travels with the fluid under the influence of various forces. For a spherical particle within the Stokes regime, the equation can be written as:

$$\frac{du_i^p}{dt} = F_D(u_{ai} - u_{pi}) + F_{\text{Saff}} + F_{\text{Virtual}} + F_{\text{P.G}} + F_{\text{Brownian}} + F_e. \quad (7)$$

F_D is drag force, F_{Saff} is Saffman force, F_{Virtual} is force due to virtual mass, $F_{\text{P.G}}$ is force due to pressure gradient, F_{Brownian} is Brownian force and F_e is electrical force.

4.3. Electrostatic field

A high negative voltage is applied to the emitting electrode at the gun-tip to generate the electrostatic field between the electrode and the grounded electrode, the coating part. The electrostatic field can be described by a Poisson equation:

$$\nabla^2 V = -\frac{\rho}{\varepsilon_0}, \quad (8)$$

where ρ is the space charge density and ε_0 is the electrical permittivity of the gas phase. The potential, V, is related to the electrostatic field intensity, E, according to:

$$\vec{E} = -\nabla V. \quad (9)$$

The space charge represents the contribution of free ions and charged particles to the overall electrostatic field. The space charge due to charged particles was not considered in this study, because earlier work [19,27] suggested that its contribution to the total space charge is 1/10th of the ionic space charge. The ionic space charge density, ρ, is related to the current density, J. With the assumption of constant ion mobility, the correlation between J and ρ can be described as:

$$\vec{J} = \mu_0 \rho \vec{E} - D\nabla\rho, \quad (10)$$

where D is the diffusion coefficient. The value of ion mobility, μ_0, can be taken from 1.82×10^{-4} m/s to 2.2×10^{-4} m/s [19,28]. The value of 2.0×10^{-4} m/s was used in this study. The current density, J, satisfies the following conservation equation:

$$\nabla.\vec{j} = 0. \quad (11)$$

Substituting Eq. (10) into Eq. (11) and combining with

Eqs. (8) and (9) yields the following partial differential equation for the space charge density:

$$D\nabla^2\rho + \mu_0 \nabla V.\nabla\rho = \frac{\rho^2\mu_0}{\varepsilon_0}. \quad (12)$$

Eqs. (8) and (12) were solved iteratively to obtain the electrostatic field. These equations were incorporated into the numerical model using the user defined scalar transport equations and user defined functions.

The Discrete Phase Model (DPM) was selected to estimate the flow of the particulate phase, since the gas-solid two-phase flow in the coating booth has been classified as a dilute flow. In DPM, the effect of particle-particle interactions on the solid flow was neglected, since the volume fraction of the solid phase is very low in the powder coating system. Also, the powder particles were considered spherical and as having smooth surfaces. The particle trajectories were predicted by integrating the equation of motion for the particles, which was based on the force balance on the particle, and written in a Lagrangian reference frame. This force balance equates particle inertia with the forces acting on the particle, and can be written (for i direction in Cartesian coordinates) as:

$$\frac{du_i^p}{dt} = F_D(u_{ai} - u_{pi}) + F_{\text{Gravity}} + F_{\text{Virtual}} + F_{\text{P.G}} + F_{Ei}/m_P, \quad (13)$$

where F_{Ei} is the electrostatic force component in the i direction, and m_p is the particle mass. The first and second terms on the right-hand side of Eq. (13) are the drag force and gravitational force, respectively. The electrostatic force, due to the electrostatic field, F_{Ei}, is given by:

$$\vec{F}_E = q_P\vec{E} + \frac{q_P^2}{16\pi\varepsilon_0 a^2}\vec{n}_P, \quad (14)$$

where q_P is the particle charge, a is the distance between the particle and the coating target, and $\vec{n_p}$ is the unit vector from the location of the particle to the point on the coating target at which the distance between the particle and the coating part is the smallest. Due to the lack of available models for the charge to mass ratio, the average value of -1$\mu c/g$, obtained from experiments, was used for the charge to mass ratio in the current study.

5. Results and discussion

5.1. Filtration efficiency

In 1987, Kanaoka et al. [10] conducted efficiency tests of split type electret filters and, accordingly, generated two semi-empirical expressions on the assumption of rectangular fibers in the vertical array arrangement (with the long side of the fiber's cross section perpendicular to the flow, as shown in Figure 1). In this paper, the results are compared with semi-empirical expressions.

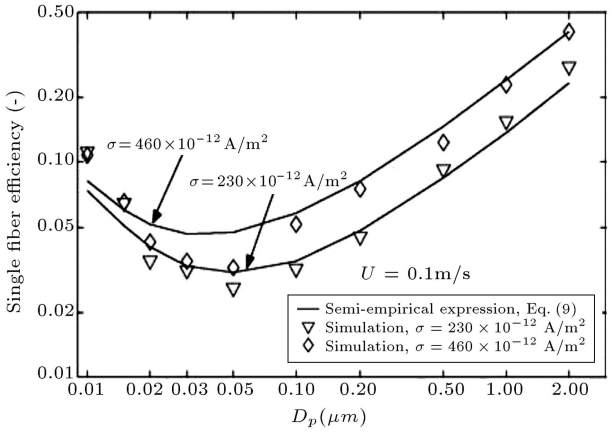

Figure 5. Single fiber efficiency of uncharged particle under various fiber charges, $U = 0.1$ m/s.

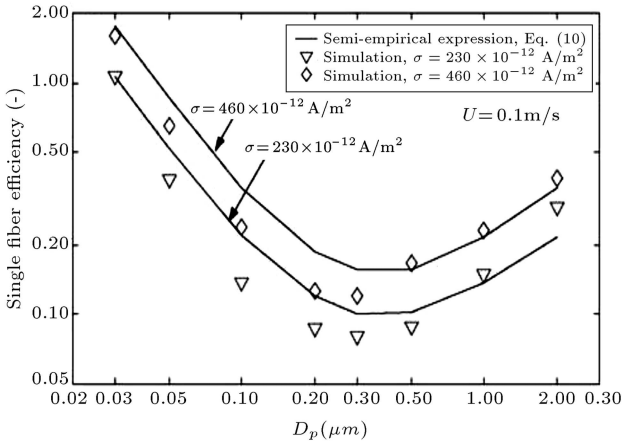

Figure 6. Single fiber efficiency of singly charged particle under various fiber charges, $U = 0.1$ m/s.

Figures 5 and 6 show the simulated single fiber efficiencies of uncharged particles and singly charged particles deposited on fibers in two charge states: 460 μ As/m^2, and half of this charge, 230 μAs/m^2. The single fiber efficiency of uncharged particles is shown in Figure 5 as a function of particle size, in which filtration velocity is 0.1 m/s and particle size is in the range of 0.01–2.0 μm. Calculated results from semi-empirical expressions are also presented in the figure as solid lines. Likewise, the single fiber efficiency of singly charged particles is shown in Figure 6. In both cases, the simulated results and those calculated from the semi-empirical expressions predicted the same trends and the two groups of results agree with each other reasonably well.

For uncharged particles, collection efficiency in Figure 5 first decreases almost linearly as particle size decreases until a minimum value is reached and then increases non-linearly with further decrease in particle size. The linear portion reflects that the

dielectrophoretic effect is dominant, while the nonlinear part reflects the effects of diffusion. There is a region of minimum single fiber efficiency on each curve, where both effects are weak. These results can be easily explained because larger particles can be polarized to a higher level and, therefore, are subjected to stronger polarization force, which will enhance capture due to the dielectrophoretic effect. On the other hand, low filtration velocity and small particle size will result in low Peclet (Pe) number, which corresponds to an intensified Brownian diffusion effect. For a singly charged particle, Figure 6 also shows the same trend. Decreases in efficiency over the particle size range 2.0-0.3 μm are caused by the weakening of the dielectrophoretic effect. The efficiency increases as particle size further decreases because the Coulombic force begins to dominate. Figures 7 and 8 show similar simulation results, except that the calculation is based on 0.5 m/s filtration velocity. Higher filtration velocity will result in a shorter resident time of a particle around the fiber, which results in generally lower electrostatic collection efficiencies. Figures 5 to 8 also show that the fiber charge greatly influences the magnitude of the efficiency, but changes very little the trend by which collection efficiency varies with particle size.

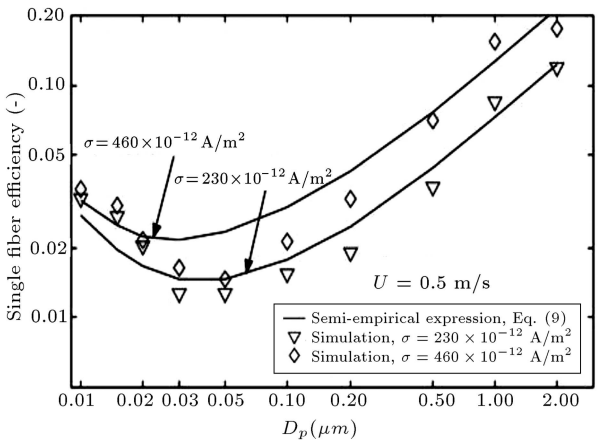

Figure 7. Single fiber efficiency of uncharged particle under various fiber charges, $U = 0.5$ m/s.

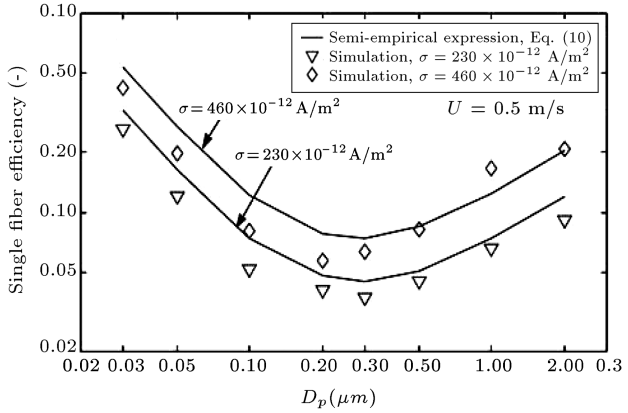

Figure 8. Single fiber efficiency of singly charged particle under various fiber charges, $U = 0.5$ m/s.

5.2. Powder coating performance

During the coating process, the grounded coating part is present in the spray zone. To check how the model behaves under conditions with and without a coating part, comparisons were made for velocities under both these conditions. This exercise also showed how the particle spray profile gets affected by the presence of the coating part.

Figures 9 and 10 show the predicted gas flow velocity vectors inside the coating booth and in the vicinity of the spray gun, respectively, with the electrostatic field and with a coating part in the coating booth. To allow a better visualization of the wake region near the spray gun deflector and the coating part, only the velocity vectors with magnitudes of 0 to 5 m/s have

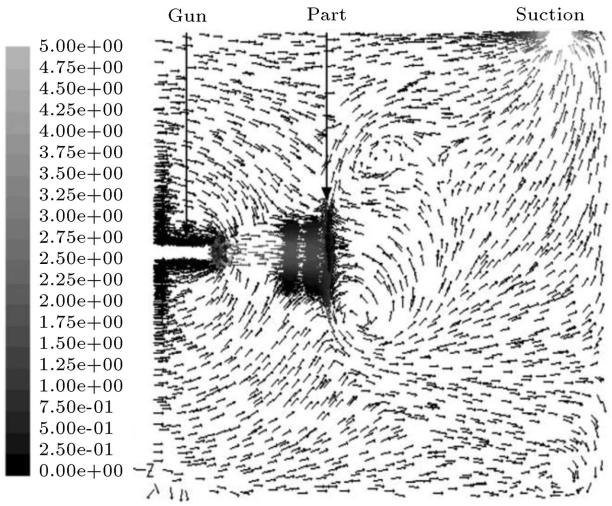

Figure 9. Gas velocity vectors inside the coating booth on the $y - z$ vertical plane at the gun.

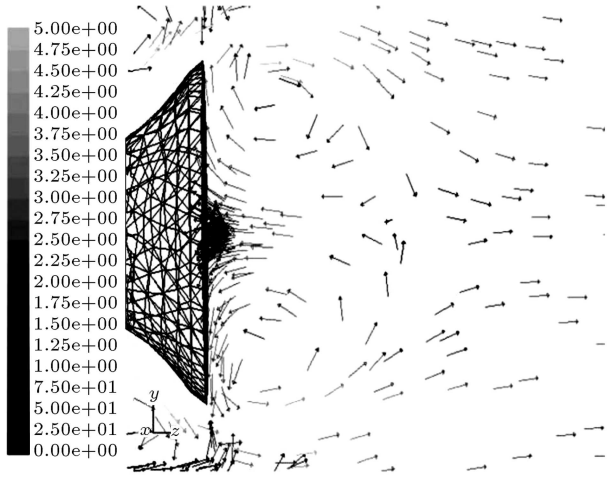

Figure 10. Gas velocity vectors in the vicinity of the gun deflector plate.

been presented in the figures. The results clearly show the wake regions near the spray gun deflector front and the coating part.

The model is also examined for its ability to predict particle velocity profiles, when a coating part is placed in the coating booth and there is no electrostatic field, by comparing the predicted results with measured values. The coating part, 7.6 cm×13.2 cm, was placed 26 cm downstream of the gun tip.

Figures 11 and 12 show the comparison between the numerical and experimental results for the velocity profiles along the vertical axis (y), 25 cm and 20 cm downstream of the gun tip. The numerical model predicted a similar pattern to that seen in the measurements. In the numerical simulation, the assumption was made that all particle hits on the coating target, stayed on the target, while, in the experiment, some particles were reflected back. In the comparison between the numerical and experimental results shown in Figures 11 and 12, all negative particle z velocities are removed from the experimental data. A discrepancy is shown in Figures 11 and 12 between the numerical results and experimental data, at 25 cm from the gun tip, which is 1 cm from the coating part. This may be related to the choice of the standard k-e turbulence model that is often not suitable for resolving flows near stagnant boundaries.

Figures 13 and 14 show a comparison for particle size distribution along the vertical axis (y), 20 and 25 cm downstream of the gun tip. The diameter distributions along the vertical axis show that the bigger particles tend to land on the bottom of the coating booth and smaller particles are at higher positions inside the coating booth. This is because bigger particles are under higher gravitational force and tend to drift downwards, while smaller particles follow the gas flow path and remain suspended for a longer time. The profile is more flat at 25 cm

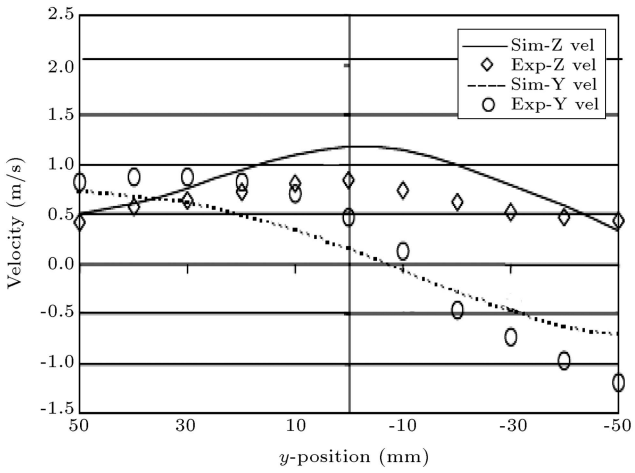

Figure 11. Particle velocity profiles along the vertical (y) axis at 25 cm downstream of the gun tip (without electrostatic field and with a coating part).

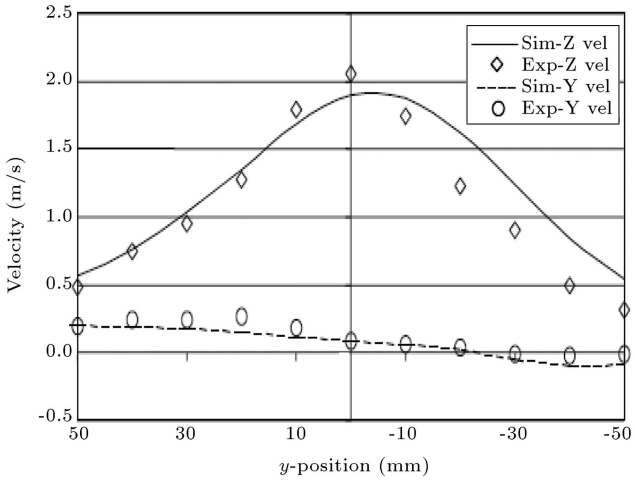

Figure 12. Particle velocity profiles along the vertical (y) axis at 20 cm downstream of the gun tip (without electrostatic field and with a coating part).

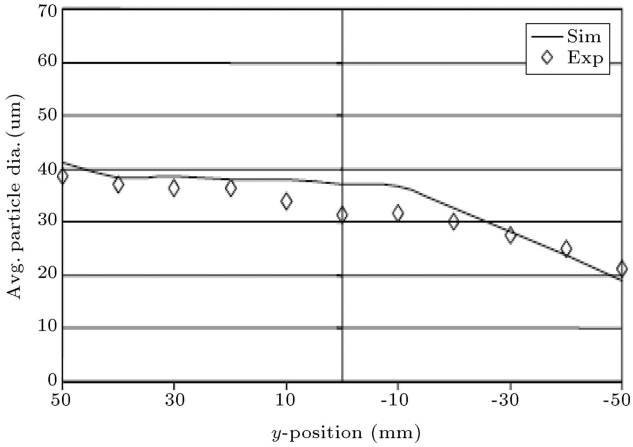

Figure 13. Particle size profiles along the vertical axis (y) at (a) 25 cm down-stream of the gun tip.

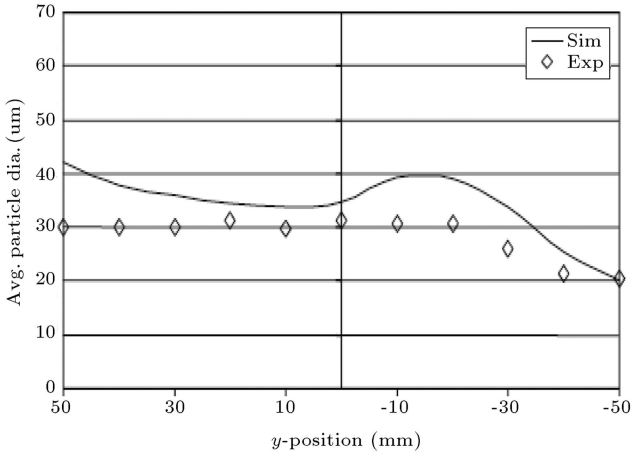

Figure 14. Particle size profiles along the vertical axis (y) at and (b) 20 cm down-stream of the gun tip.

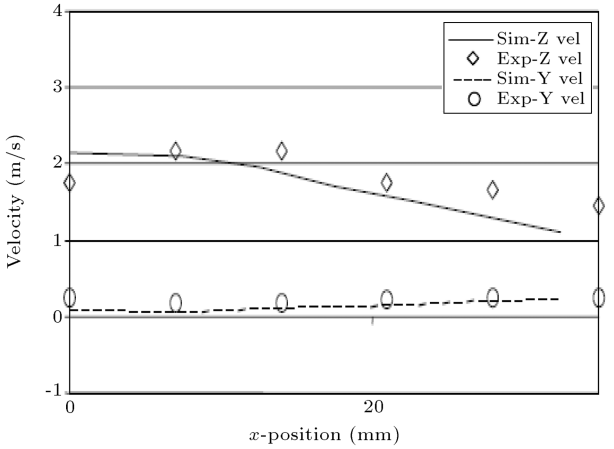

Figure 15. Particle velocity profiles along the horizontal axis (x) at 20 cm downstream of the gun tip (with electrostatic field and with coating part).

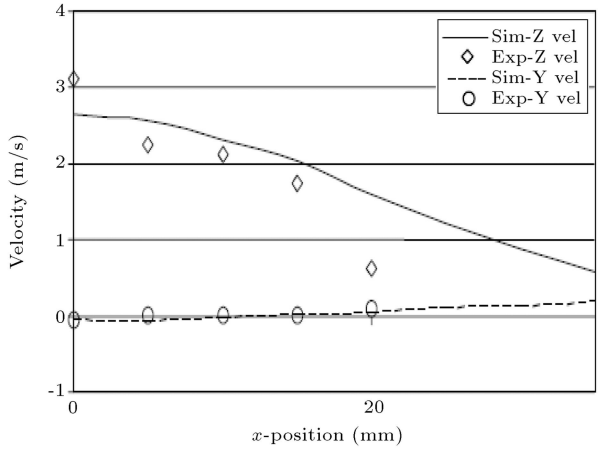

Figure 16. Particle velocity profiles along the horizontal (x) axis 10 cm downstream of the gun tip (with electrostatic field and with coating part).

than it is at 20 cm, because many big particles have fallen down. Both figures show good agreement between the predicted results and the experimental data.

Figures 15 and 16 show a comparison of particle velocities along the horizontal axis (x), 20 cm and 10 cm downstream of the gun tip, for the case with a coating part in the coating booth and with an electrostatic field. These figures show a reasonable agreement between the numerical results and experimental data for both z and y velocities, except for the z velocity at $x = 20$ mm and 10 cm from the gun tip, where the experimental value is much lower than the simulation value, as shown in Figure 16. The comparison 25 cm downstream of the gun tip, which is very close to the part, was not made, since back ionization affects experimental data for particle velocities very close to the coating part, and the numerical model used here does not account for its effect.

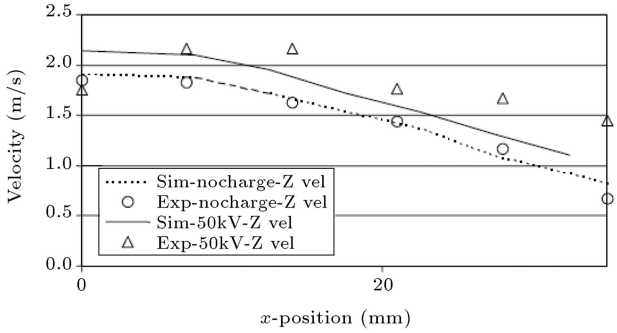

Figure 17. Particle velocity profiles with and without electrostatic field on the horizontal (x) axis at 20 cm downstream of the gun tip (with coating part).

Particle velocity profiles with an electrostatic field were compared with those without an electrostatic field to understand the effect of the applied electrostatic field on particle motion and the trajectories of the particle. Figure 17 shows the comparison along the horizontal (x) axis, 20 cm downstream of the gun tip. It shows that the electrostatic field causes an increase in particle velocity towards the coating part, i.e. an increase in z velocity.

6. Conclusions

In this paper, the charged and neutral particle collections in an electret filter composed of rectangular split-type fibers are simulated. Both the flow field and the electric field around the fiber are numerically determined. All major collection mechanisms, mechanical and electrostatic, have been coupled in the differential equation forms of particle motion. Simulations have been conducted under a wide range of filtration conditions, and results are compared with those obtained from experiments.

Single fiber collection efficiency is obtained from tracing and recording particle trajectories. For the uncharged particles and singly charged particles deposited on fibers in two charge states: 460 μ As/m^2 and 230 μ As/m^2, as a function of particle size, two filtration velocities of 0.1 m/s and 0.5 m/s were studied. The particle size was within the range of 0.01-2.0 μm. Numerical models for simulations of gas and solid particle flows in an electrostatic powder coating system are presented. For an uncharged particles with 0.1 m/s speed, the minimum efficiency corresponds to particle size of $0.05 \mp m$, and the effect of electrical charge is less pronounced for smaller size particles. However, the overall trend agrees well with experiments. For charged particles with 0.1 m/s speed, the minimum efficiency relates to larger particle size of $0.3 \mp m$, whilst, the overall trends better predicts experiments, particularly the electrical charge effects. In both cases, the computational results are slightly underestimated

compared to experiments. Similar trends are observed when a higher speed of 0.5 m/s is adopted.

The distribution of powder particle velocities indicates that the numerical model predicts, quite accurately, particle velocity and average particle diameter at different locations inside the coating booth, up to 20 cm away from the gun tip. The numerical results showed a similar effect of the electrostatic field on the flow field, to that of experimental results. The differences between numerical results and experimental data at longer distances, for the case of with a coating part and an electrostatic field, are most probably due to the assumption of constant charge to mass ratio and the spherical shape of particles in this study. To improve this, it may be useful to numerically resolve particle charging using unsteady particle tracking, or alternatively, consider variable particle charge based on its diameter.

For further scope of the present study, it is suggested to extend the simulation of particles in the electromagnetic field in bio-inspired subjects, such as the movement of microorganisms, like paramecium in a fluid medium. These microorganisms change their swimming orientations due to application of an external magnetic or electric field, and it is believed that these microorganisms can be used instead of micro robots for in-vivo therapies. The discussed method of simulations here may be extended for the creeping motion of such bio organisms as micro particles.

References

1. Welling, I., Lehtimäki, M., Rautio, S., Lähde, T., Enbom, S., Hynynen, P. and Hämeri, K. "Wood dust particle and mass concentrations and filtration efficiency in sanding of wood materials", *Journal of Occupational and Environmental Hygiene*, **6**(2), pp. 90-98 (2008).
2. Leung, W.W.F., Hung, C.H. and Yuen, P.T. "Experimental investigation on continuous filtration of submicron aerosol by filter composed of dual-layers including a nanofiber layer", *Aerosol Science and Technology*, **43**(12), pp. 1174-1183 (2009).
3. Li, K. and Jo, Y.M. "Dust collection by a fiber bundle electret filter in an MVAC system", *Aerosol Science and Technology*, **44**(7), pp. 578-587 (2010).
4. Quadrini, F., Santoa, L., Tagliaferria, V. and Trovaluscia, F. "Custom painting by means of powder coating and localized heating", *Polymer-Plastics Technology and Engineering*, **49**(2), pp. 164-168 (2010).
5. Sultana, Z.M., Nilssona, G.J. and Mageea, R.J. "Removal of ultrafine particles in indoor air: Performance of various portable air cleaner technologies", *HVAC & R Research*, **17**(4), pp. 513-525 (2011).
6. Atsushi Tanaka, Tuomo Hjelt, Asko Sneck, and Antti Korpela "Fractionation of nanocellulose by foam filter", *Separation Science and Technology*, **47**(12), pp. 1771-1776 (2012).
7. Baumgartner, H.P. and Löffler, F. "The collection performance of electret filters in the particle size range 10 nm-10 J μm, *J. Aerosol Sci.*, **17**, pp. 438-445 (1986).
8. Baumgartner, H., Piesch, C. and Umhauer, H. "High-speed cinematographic recording and numerical simulation of particle depositing on electret fibers", *J. Aerosol Sci.*, **24**, pp. 945-962 (1993).
9. Cao, Y.H., Cheung, C.S. and Yan, Z.D. "Numerical study of an electret filter composed of an array of staggered parallel rectangular split-type fibers", *Aerosol Science and Technology*, **38**(6), pp. 603-618 (2004).
10. Kanaoka, C., Emi, H., Otani, Y. and Ishiguro, T. "Effect of charging state of particles on electret filtration", *Aerosol Sci. Technology*, **7**, pp. 1-13 (1987).
11. Kanaoka, C. "Performance of an air filter at dust-loaded condition", In *Adv in Aerosol Filtration*, Edited by Spurny, K.R., Chapter 16, Lewis Publishers (1998).
12. Kanaoka, C. and Hiragi, S. and Tanthapanichakoon, W. "Stochastic simulation of the agglomerative deposition process of aerosol particles on an electret fiber", *Powder Technology*, **118**, pp. 97-106 (2001).
13. Romay, F.J., Liu, B.Y.H. and Chae, S.J. "Experimental study of electrostatic capture mechanisms in commercial electret filters", *Aerosol Sci. Technol.*, **28**, pp. 224-234 (1998).
14. Brown, R.C. "Electric effects in dust filters", *In Proc. 2nd World Filtration Congress*, London, pp. 291-301 (1979).
15. Brown, R.C. "Capture of dust particles in filters by line-dipole charged fibers", *J. Aerosol Sci.*, **12**, pp. 349-356 (1981).
16. Oh, Y.W., Jeon, K.J., Jung, A.I. and Jung, Y.W. "Simulation study on the collection of submicron particles in a unipolar charged fiber", *Aerosol Sci. Technol.*, **36**, pp. 573-582 (2001).
17. Böttner, C.U. and Sommerfeld, M. "Numerical calculation of electrostatic powder painting using the Euler/Lagrange approach", *Powder Technology*, **125**(2), pp. 206 -217 (2002).
18. Ye, Q., Steigleder, T., Scheibe, A. and Domnick, J. "Numerical simulations of the electrostatic powder coating process with a corona spray gun", *J. Electrostat.*, **54**, pp. 189-205 (2002).
19. Ye, Q. and Domnick, J. "On the simulation of space charge in electrostatic powder coating with a corona spray gun", *Powder Technol.*, pp. 250-260 (2003).
20. Li, Z., Zhang, C. and Zhu, J. "Numerical study of air-particle two-phase flows inside a powder coating booth", *International Journal for Computational Methods in Engineering Science and Mechanics*, **7**(3), pp. 141-154 (2006).
21. Juberya, T.Z. and Dutta, P. "A fast algorithm to predict cell trajectories in microdevices using dielectrophoresis", *Numerical Heat Transfer, Part A: Applications: An International Journal of Computation and Methodology*, **64**(2), pp. 107-131 (2013).

22. Fardi, B. and Liu, B.Y.H. "Flow field and pressure drop of filters with rectangular fibers", *Aerosol Sci. Technol.*, **17**, pp. 36-44 (1992a).

23. Fardi, B. and Liu, B.Y.H. "Efficiency of fibrous filters with rectangular fibers", *Aerosol Sci. Technol.*, **17**, pp. 45-58 (1992b).

24. Chen, S., Cheung, C.S., Chan, C.K. and Zhu, C. "Numerical simulation of aerosol collection in filters with staggered parallel rectangular fibers", *Comput. Mech.*, **28**, pp. 152-161 (2002).

25. Rao, N. and Faghri, M. "Computer modeling of electrical enhancement in fibrous filters", *Aerosol Sci. Technol.*, **13**(2), pp. 127-134 (1990).

26. Emi, H., Otani, Y. and Ishiguro, T. "Effect of charging state of particles on electret filtration", *Aerosol Sci. Technology*, **7**, pp. 1-13 (1987).

27. Bailey, A.G. "The science and technology of electrostatic powder spraying transport and coating", *J. Electrostat.*, **45**, pp. 85-120 (1998).

28. Anagnostopoulos, J. and Bergeles, G. "Corona discharge simulation in wire-duct electrostatic precipitator", *J. Electrostat.*, **54**, pp. 129-147 (2002).

Biographies

Ahmad Sedaghat has been an Assistant Professor at Isfahan University of Technology since 2004. He obtained his PhD Degree in Aerospace Engineering from the University of Manchester in 1997. He has undertaken various postdoctoral research fellowships, including: 1998, Leuven University, Belgium, on the MMARIE European project; 1998 to 2001, the University of Manchester, with BAE Systems in Nonlinear Aeroelasticity; 2001 to 2004, the University of Leeds, with the British Combustion Institute, in Combustion Instabilities; and 2008 to 2009, the University of Central Lancashire, with the Joule Centre for energy research & development, in Innovative Small Wind Turbines. He is currently working in the field of renewable energy and the aerodynamic/aeroelasticity of wind turbines.

Amir Hossein Mohammadzadeh obtained his MS degree from the Department of Mechanical Engineering at Isfahan University of Technology, Iran, in 2010, and is currently Chief Operational Engineer at Shahid Montazeri power plant in Isfahan, Iran.